

Electrostatic probe diagnostics of a planar-type radio-frequency inductively coupled oxygen plasma

D. C. Seo, T. H. Chung,^{a)} and H. J. Yoon
Department of Physics, Dong-A University, Pusan 604-714, Korea

G. H. Kim
Department of Physics, Hanyang University, Ansan, Kyunggido, 425-791, Korea

(Received 1 August 2000; accepted for publication 16 January 2001)

An inductively coupled oxygen radio-frequency (13.56 MHz) discharge is investigated based on modeling and experiment. Experimental measurement is done at a range of gas pressure of 1–30 mTorr, and rf power of 100–1000 W. We measure most of the important plasma parameters such as the densities of charged species, electron temperature, plasma potential, and electron energy distribution function. The measured values are compared with the results of the spatially averaged global model. We observe a generally good agreement between the modeling and the experiment. The scaling features, the transition of the operating region, and the radial distributions of charged species are also discussed. © 2001 American Institute of Physics. [DOI: 10.1063/1.1354633]

I. INTRODUCTION

Oxygen plasmas have found numerous applications in plasma processing such as plasma-enhanced chemical-vapor deposition, reactive sputtering, dry etching of polymer, oxidation, and resist removal of semiconductors. Negative ions are found in electronegative gases such as oxygen, chlorine, and fluorocarbons, which are used extensively in discharges for various applications of plasma processing.

The presence of negative ions complicates the discharge phenomena. Negative-ion sources can be applied to charging-free-ion implantation in semiconductor manufacture, and negative-ion-assisted etching is found to reduce the charging of substrates.¹ There is considerable scientific and technological interest in electronegative plasmas,^{2–6} and so in the determination of negative-ion density.^{7–9}

Langmuir probes, mass spectrometry, ion acoustic wave, and optogalvanic photodetachment are usual methods for investigating negative ions in plasma.¹⁰ Negative-ion-containing plasmas are generated in a variety of energy-coupling methods such as dc,¹¹ rf capacitive,¹² rf inductive,^{7,8} and hollow cathodes^{13,14} discharges.

There has been an increased demand to understand the scaling of the plasma constituents with control parameters for such multicomponent systems. The scaling of plasma variables (charged-particle densities, sheath width, electron temperature, and plasma potential) with the operating parameters gives useful information for the design and analysis of plasma sources. The operating regions were classified in the entire control parameter space.¹⁵ The discharge properties such as the ratio of the negative-ion density to the electron density, the spatial profile of charged species, and the prevailing particle loss mechanism (volume recombination loss or ion flux loss to the wall due to diffusion) also depend on the operating region. Thus, in various regions, the discharge

generally exhibits different scalings of the operating parameters.

In a previous article,¹⁶ we explored the scaling relations for a low-power region, and observed that the experimentally measured scalings of the charged species are in agreement with the predictions of the spatially averaged global model. We observed the scaling laws to hold in a medium power region.¹⁷

In this article, we measure most of the important plasma parameters such as the densities of charged species, electron temperature, plasma potential, and electron energy distribution function over the range of pressure and power that is typical of those used currently in the industry. The measured values are compared with the results of the global model. Specifically, we investigate the scaling features and the transition of the operating region for a low-pressure inductively coupled oxygen plasma in normal operating regions of several hundred watt power. Along with that, we perform the measurement of the radial distribution of the charged species in the chamber which indicates the level of uniformity in a processing reactor.

II. EXPERIMENT

The plasma chamber consists of a stainless-steel cylinder with a 28 cm diam and 34 cm length. A 1.9-cm-thick by 27-cm-diam tempered glass plate mounted on one end separates the planar one-turn induction coil from the plasma. Figure 1 shows a schematic of the planar inductive plasma source and Langmuir probe diagnostics system. A disk-type Langmuir probe made of tungsten with a single side of 6 mm diam is located 11 cm from the window on the axis of the chamber to measure the floating and plasma potentials, positive and negative saturation current, and electron temperature.

The plasma chamber is evacuated by a diffusion pump backed by a rotary pump giving a base pressure of 10^{-5} Torr. The equilibrium gas pressure in the chamber is moni-

^{a)}Electronic mail: thchung@plasma.donga.ac.kr

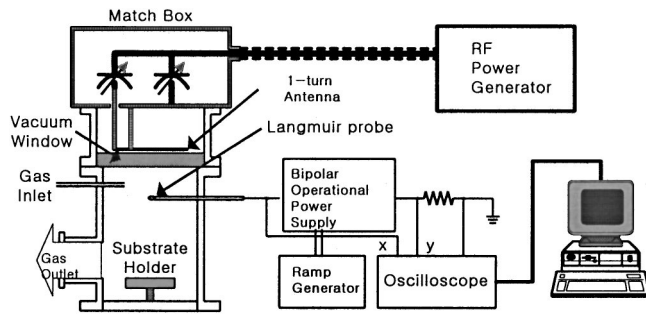


FIG. 1. Schematic of a planar inductively coupled plasma source and Langmuir probe diagnostics system.

tored with a penning gauge. The operating gas pressure is controlled by adjusting the mass flow controller (AFC 50). The flow rate of the oxygen gas has a range of 10–20 sccm. The oxygen gas pressure is varied in the range 1–30 mTorr. The induction coil is made of copper (with water cooling) and connected to an L-type capacitive matching network and a rf power generator (ENI OEM-12).

The Langmuir probe is powered by a Kepco bipolar operational power supply amplifier. A triangle ramp wave, swept from –50 to +50 V at 300 Hz is fed into the Kepco from a homemade ramp generator. The current measurement is done across a 200 Ω resistor placed between the common and ground outputs of the Kepco amplifier. The current and voltage signals are collected on a HP54645A digitizing oscilloscope.

Experiments were conducted at several pressures and powers. In order to allow the chamber to reach an equilibrium, the plasma was turned on and allowed to run for an hour before taking any measurements. We consider a relatively simple Langmuir probe technique to estimate the negative-ion density. The results of the Langmuir probe measurements are compared with the results of the global model.

The second derivative of the measured probe current, I'' , is related to the electron energy distribution function (EEDF), $f(\epsilon)$, as follows:

$$f(\epsilon) = \frac{2m}{e^2 S} \left(\frac{2eV}{m} \right)^{1/2} I'' \tag{1}$$

where e is the electronic charge, S is the probe area, m is the mass of the electrons, V is the probe potential referenced to the plasma potential, and ϵ is measured in units of eV. The electron density and the effective electron temperature are calculated with the measured EEDF as follows:

$$n_e = \int_0^{\epsilon_{\max}} f(\epsilon) d\epsilon, \quad T_{\text{eff}} = \frac{2}{3n_e} \int_0^{\epsilon_{\max}} \epsilon f(\epsilon) d\epsilon, \tag{2}$$

where ϵ_{\max} is determined by the dynamic range of the EEDF measurement. The electron temperature can also be determined from the slope of the probe $\ln(I) - V$ curve in the exponential region (from the point where the probe current is zero to where the slope of the curve begins to decrease). We observe that the both methods yield almost the same values.

The positive-ion saturation current is

$$I_+ = 0.6eSn_+ \left(\frac{T_e}{M_+} \right)^{1/2}, \tag{3}$$

where n_+ is the positive-ion density and M_+ is the positive-ion mass. It is assumed that the Bohm criterion for the formation of a stable sheath holds even if negative ions exist. In estimating the ion saturation current, the edge effects are considered by considering the correction equation.¹⁸

We have a density balance between negatively and positively charged particles given by $n_e + n_- = n_+$. By measuring the positive-ion saturation current, one can estimate the densities of positive ions and negative ions. This method has the advantage of avoiding determining the negative-ion temperature.

It is known that the abundance of the atomic positive ion O^+ depends on the surface recombination rate, gas pressure, and absorbed power. In this study, we assume that O_2^+ is the major positive ion, O^- is the major negative ion, and that the oxygen molecules are far from being completely dissociated, due to a very high oxygen atom recombination frequency on the reactor walls.¹⁹ However, it has been found that the degree of dissociation increases with the rf power. O_2^- ions are produced by charge-transfer processes in the collision of O^- ions with O_2 . The O_2^- density is known to be much smaller than the O^- density in the operating region of this study.

We have compared the measured values to those calculated by a spatially averaged global model. The set of the main reactions, the reaction coefficients, and the formulations are found in our previous study.¹⁶ The rate constants, which have a critical influence on the formation of negative ions, are based on the work of Lee and co-workers,^{2,3} Eliasson and Kogelschatz,²⁰ and Panda, Economou, and Meyyappan.²¹ One difference is that in this study the sheath potential V_s is determined by equilibrium fluxes of positive and negative species to the wall instead of $V_s = T_e/2 \ln(M_{O_2}/2\pi m)$. Another thing is that this study uses the h_L and h_R factors, which are the ratios of sheath edge positive densities (axial and radial) to those in the bulk plasma according to those suggested by Lee and Lieberman.²

III. RESULTS AND DISCUSSION

Figure 2 shows the positive-ion density as a function of pressure. The variation of the positive-ion density with pressure is in agreement with the other experimental results.^{22–24} We observe that the positive-ion density increases with pressure at a low-pressure range, has a maximum, and then decreases slightly. This behavior seems to be related to the transition of the dominant loss mechanism of charged particles in electronegative plasmas. In the low-pressure range, the dominant loss of charged particles is due to diffusion (we call this range the ion-flux-loss-dominated region), while in the medium- or high-pressure range, the loss takes place mainly via the volume recombination (the recombination-loss-dominated region). The increase of the volume recombination makes the charged-particle density decrease with pressure since the more charged particles a discharge produces the more recombination it results in. The increase of recombination loss along with the diffusion loss makes the

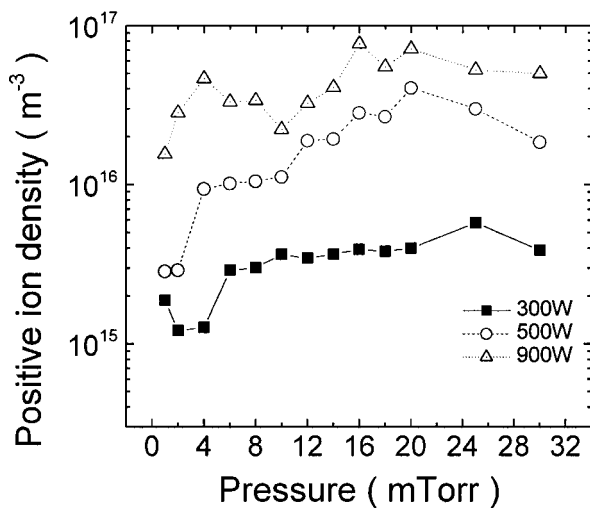


FIG. 2. Positive-ion densities as a function of pressure for $P_{\text{abs}}=300, 500, 700,$ and 900 W.

charged-particle density decrease. This behavior was also observed in a pulsed oxygen discharge.²¹ The simulation of Shibata, Nakano, and Makabe²⁵ showed a peak on the O_2^+ (dominant positive ion) density and the experiment of capacitively coupled oxygen discharge done by Stoffels *et al.*²⁶ showed a peak in the electron density with pressure. From Fig. 2, we can note that the transition from the ion-flux-loss-dominated region to the recombination-loss-dominated region takes place at a specific value of pressure. The origin of this transition and the scaling laws at each operating region were fully discussed in our previous paper.¹⁶

The transition points are about 26 mTorr for 300 W inductive power, 20 mTorr for 500 W power, and 16 mTorr for 900 W power. The transition point moves to a lower pressure value as the absorbed power increases. This can be accounted for by considering that enough positive and negative ions which are produced in higher-power conditions make the recombination loss dominant at lower pressure.

Figure 3 shows the comparison of the negative-ion density between the results of the global model and the experi-

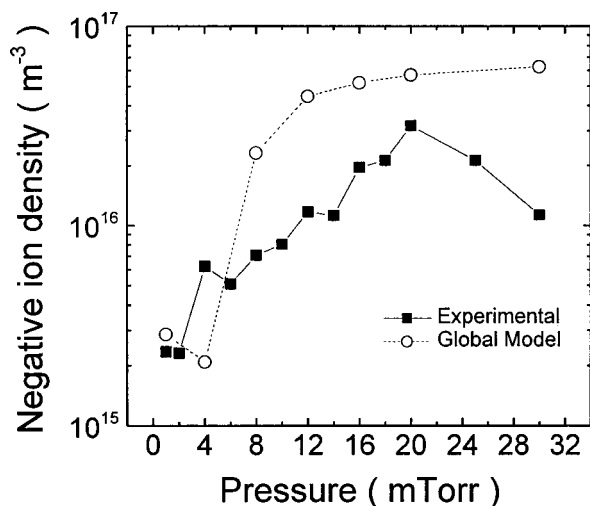


FIG. 3. Negative-ion densities as a function of pressure for $P_{\text{abs}}=500$ W.

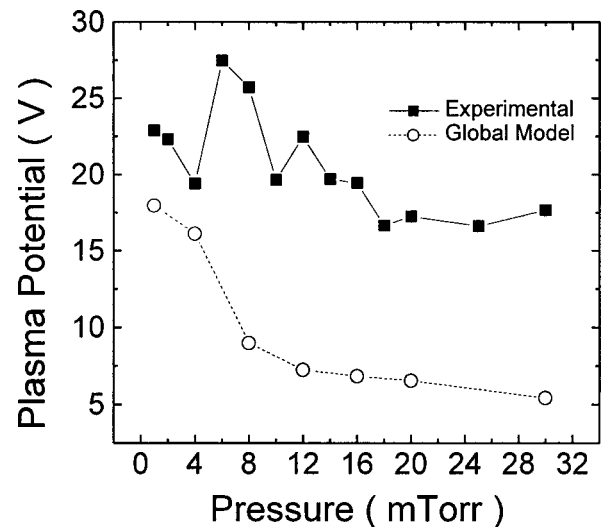


FIG. 4. Plasma potential as a function of pressure. Comparison is made between experimental values and calculated values. Here, $P_{\text{abs}}=500$ W.

mental results. The negative-ion density rises with increasing pressure up to 20 mTorr, and this is also in agreement with the experimental results. The residence time of negative ions in the chamber can be estimated from the gas pressure, flow rate, and chamber size. The estimated residence time is about 2.5 s. The reason for the substantial formation of negative ions in this short period of stay is that negative ions are produced via a variety of mechanisms which include the dissociative attachment of low-energy electrons to the metastable and excited oxygen molecules.^{21,27} In the pulsed-mode operation of oxygen discharge with a gas pressure and flow rate comparable to those of this study, a negative-ion density in the order of 10^{11} cm^{-3} was observed.^{8,27} However, the global model does not explain that the negative-ion density has a maximum which indicates the transition of the operating region.

In Fig. 4, the calculated and measured plasma potential are shown with varying pressures. The experimental results are obtained from measurements done at 500 W inductive power. The discrepancy may be due to it being very difficult to determine the plasma potential from the probe $I-V$ curve for the negative-ion-containing plasma. In this study, we determine the plasma potential by the value of the probe voltage where the second derivative of the probe current vanishes. The presence of negative ions complicates the characteristics of the probe $I-V$ curve. Negative ions contribute to the probe current in the exponential region, and the amount of the contribution gets larger when the probe voltage approaches the plasma potential. In addition, the fluctuation of the collected probe current due to rf oscillation makes the $I-V$ curve difficult to interpret.

Although not shown in the figures, the behavior of the ratio of the negative ions to the electron density is qualitatively consistent with the experimental results by Tuszewski²⁸ and Gudmundsson.²⁹ The ratio increases with increased pressure, and decreases with increased power.

Figure 5 shows electron temperature as a function of pressure at input powers of 300, 500, 700, and 900 W. A

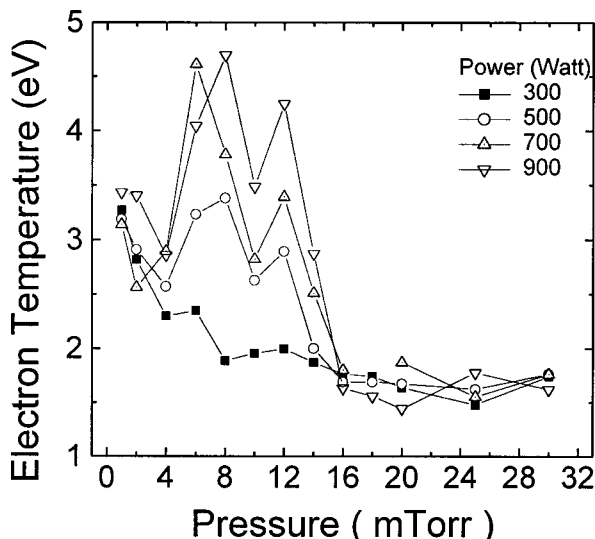


FIG. 5. Electron temperature as a function of pressure at several input powers of 300, 500, 700, and 900 W.

decrease in electron temperature with increasing pressure is typical and is in agreement with the previously reported results. However, for relatively higher powers, there exists a region around 10 mTorr where the electron temperature becomes quite large. We can note that over the region of 7–15 mTorr the electron temperature increases when the input power is increased. This behavior has been recently reported.³⁰ This can provide a significant implication for the plasma-induced damage because the damaging dose into the thin gate oxide increases with both electron temperature and plasma density.

The main causes of the increase of electron temperature with increasing power are the increase of the effective activation energy for ionization and the heating of the gas (and the resulting decrease in the neutral number density). The former is reflected in the results obtained by the global modeling, as in Fig. 6. But, this effect is not dominant. The latter seems more influential and is related to the neutral particle

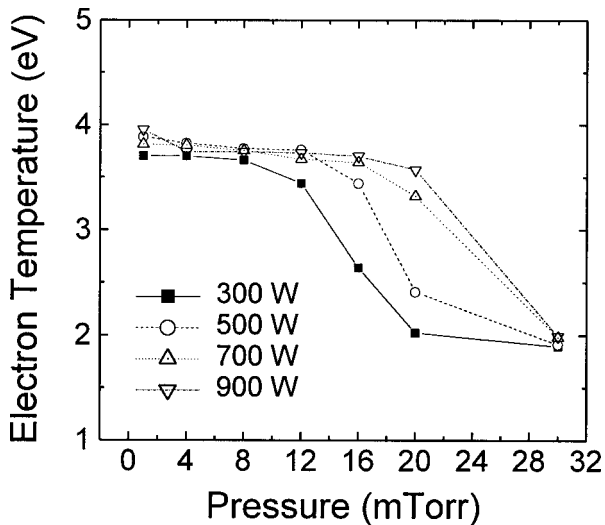


FIG. 6. Calculated electron temperature as a function of pressure. Here, the surface recombination coefficient is 0.05.

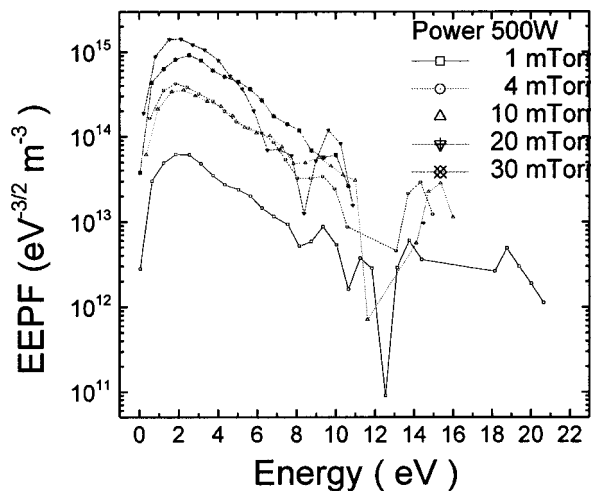


FIG. 7. Electron energy probability function (EEPF) at 500 W input power.

depletion. It was observed by Tynan³¹ that below 10 mTorr the neutral depletion is proportional to the gas pressure and above 10 mTorr the depletion is inversely proportional to the gas pressure, and that higher power results in severe depletion. These observations are in agreement with the results shown in Fig. 5.

Figure 7 shows the EEPF at several pressures at an input power of 500 W. We can observe that at low pressure, the EEPF is close to a Maxwellian. The 4 and 10 mTorr distributions are somewhat bi-Maxwellian over the region of 2–12 eV. The effective electron temperature has different trends for collisional and stochastic heating-dominated regimes. The effective electron temperature in the collision-dominated regime (20 and 30 mTorr) decreases slightly with increasing pressure and input power. Quite oppositely, for the stochastic heating-dominated regime (1 and 4 mTorr), the effective electron temperature grows slightly with increasing pressure and input power. These can be observed directly in Fig. 5. This behavior was also observed in capacitively coupled rf discharges.³²

Figure 8 is the same figure at the input power of 700 W. The EEPF above 8 mTorr increasingly deviates from the Maxwellians. EEPFs above 10 mTorr show much sharper

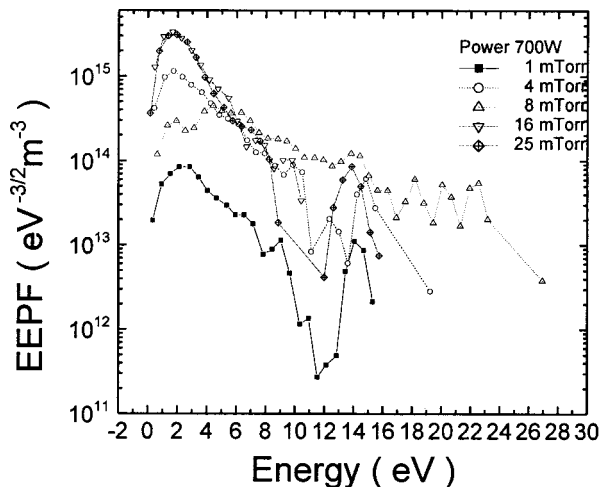


FIG. 8. Electron energy probability function at 700 W input power.

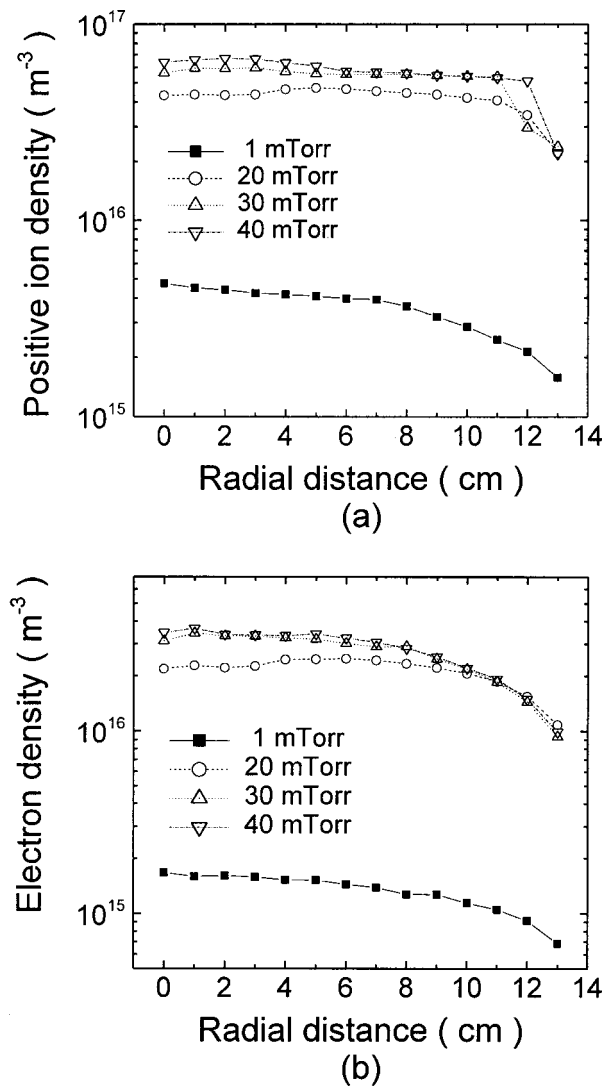


FIG. 9. Radial distributions of (a) positive ions and (b) electron densities at several pressures. The input power is 500 W.

and more pronounced peaks at low energies ($\epsilon < 5$ eV), which indicates that the EEPF changes from a single-temperature Maxwellian to a two-temperature structure (bi-Maxwellian), and the EEPF is depleted at high energies due to the inelastic interaction as well as the escape of high-energy electrons from the bulk to the chamber walls.³³ Further increases in the input power lead to an abrupt change in the EEPF shape with a drop in the effective electron temperature and a rapid increase in plasma density.

Figures 9(a) and 9(b) represent the experimentally obtained radial distributions of positive ions and electrons at different pressures. We note that the positive ions have flat-top profiles at relatively higher pressures and that with decreasing pressure the profile becomes parabolic, in accordance with the theoretical prediction.⁶ For all the pressure cases, the radial distribution of electrons follows the solution of the diffusion equation. Also, we note that the lower pressure case has a smoother character, which was also observed in oxygen dc glow discharges.¹¹ In this experiment, the electronegative core region is hardly defined, contrary to the theoretical prediction.⁶

IV. CONCLUSION

Electronegative inductively coupled oxygen rf discharges have been studied based on Langmuir-probe measurements and the results are compared with a spatially averaged global model. The charged-particle densities, the electron temperature, the plasma potential, and the electron energy probability function are obtained and the behaviors of these parameters are discussed. The experiment and the modeling are over all in agreement except that the global model predicts more or less overestimated quantities of the charged-particle densities. A transition from the ion-flux-loss-dominated region to the recombination-loss-dominated region around $p = 20\text{--}40$ mTorr is observed. Each region has a different scaling of plasma variables, which proves to be in a good qualitative agreement with the predictions of the global model.¹⁶ The effective electron temperature has different trends for collisional and stochastic heating-dominated regimes. The effective electron temperature in the collision-dominated regime (which corresponds to the recombination-dominated region from the view point of the particle-loss mechanism) decreases slightly with increasing pressure and input power. Quite oppositely, for the stochastic heating-dominated regime (which corresponds to the ion-flux-loss-dominated region), the effective electron temperature grows slightly with increasing pressure and input power. It is observed that the positive ions have flat-top profiles at relatively higher pressures (recombination-loss-dominated region) and that with decreasing pressure the profile becomes parabolic. For all the pressure cases, the radial distribution of electrons is similar to the solution of the diffusion equation.

ACKNOWLEDGMENTS

The authors are grateful to Professor A. J. Lichtenberg and Professor M. A. Lieberman of the University of California at Berkeley for fruitful discussions. This work is supported by Research Fund of Dong-A University and Hanbit User Program of Korea Basic Science Institute.

- ¹S. Samukawa and T. Mieno, *Plasma Sources Sci. Technol.* **5**, 132 (1996).
- ²C. Lee and M. A. Lieberman, *J. Vac. Sci. Technol. A* **13**, 368 (1995).
- ³C. Lee, D. B. Graves, M. A. Lieberman, and D. W. Hess, *J. Electrochem. Soc.* **141**, 1546 (1994).
- ⁴Y. T. Lee, M. A. Lieberman, A. J. Lichtenberg, F. Bose, H. Baltes, and R. Patrick, *J. Vac. Sci. Technol. A* **15**, 113 (1997).
- ⁵M. A. Lieberman and S. Ashida, *Plasma Sources Sci. Technol.* **5**, 145 (1996).
- ⁶T. H. Chung, *J. Korean Phys. Soc.* **34**, 24 (1999).
- ⁷E. Quandt, H. F. Fobele, and W. G. Graham, *Appl. Phys. Lett.* **72**, 2394 (1998).
- ⁸D. Hayashi and K. Kadota, *J. Appl. Phys.* **83**, 697 (1998).
- ⁹H. J. Yoon, T. H. Chung, and D. C. Seo, *Jpn. J. Appl. Phys., Part 1* **38**, 6890 (1999).
- ¹⁰M. Vucelic and S. Mijovic, *J. Appl. Phys.* **84**, 4731 (1998).
- ¹¹V. V. Ivanov, K. S. Klopovsky, D. V. Lopaeu, A. T. Rakhimov, and T. V. Rakhimova, *IEEE Trans. Plasma Sci.* **27**, 1279 (1999).
- ¹²H. Amemiya and N. Yasuda, *J. Phys. Soc. Jpn.* **66**, 623 (1997).
- ¹³H. Amemiya and K. Ogawa, *J. Phys. D* **30**, 879 (1997).
- ¹⁴W. Ding, D. L. Dennis, L. McCorkle, and L. A. Pinnaduwa, *J. Appl. Phys.* **84**, 3051 (1998).
- ¹⁵A. J. Lichtenberg, M. A. Lieberman, I. G. Kouznetsov, and T. H. Chung, *Plasma Sources Sci. Technol.* **9**, 45 (2000).
- ¹⁶T. H. Chung, H. J. Yoon, and D. C. Seo, *J. Appl. Phys.* **86**, 3536 (1999).

- ¹⁷T. H. Chung, D. C. Seo, G. H. Kim, and J. S. Kim, *IEEE Trans. Plasma Sci.* (submitted).
- ¹⁸J. D. Johnson and A. J. T. Holms, *Rev. Sci. Instrum.* **61**, 2628 (1990).
- ¹⁹A. Granier, F. Nicolazo, C. Vallee, A. Gouillet, G. Turban, and D. Groll-eau, *Plasma Sources Sci. Technol.* **6**, 147 (1997).
- ²⁰B. Elliasson and U. Kogelschatz, Brown Boveri Report No. KLR 86-11 C (1986).
- ²¹S. Panda, D. J. Economou, and M. Meyyappan, *J. Appl. Phys.* **87**, 8323 (2000).
- ²²J. H. Keller, J. C. Forster, and M. S. Barns, *J. Vac. Sci. Technol. A* **11**, 2487 (1993).
- ²³M. S. Barns, J. C. Forster, and J. H. Keller, *Appl. Phys. Lett.* **62**, 2622 (1993).
- ²⁴Y. Ra and C. H. Chen, *J. Vac. Sci. Technol. A* **11**, 2158 (1996).
- ²⁵M. Shibata, N. Nakano, and T. Makabe, *J. Appl. Phys.* **80**, 6142 (1996).
- ²⁶E. Stoffels, W. W. Stoffels, D. Vender, M. Kando, G. M. W. Kroesen, and F. J. de Hoog, *Phys. Rev. E* **51**, 2425 (1995).
- ²⁷D. Hayashi and K. Kadota, *Jpn. J. Appl. Phys., Part 1* **38**, 225 (1999).
- ²⁸M. Tuszewski, *J. Appl. Phys.* **79**, 8967 (1996).
- ²⁹J. T. Gudmundsson, Ph.D. thesis, University of California at Berkeley (1996).
- ³⁰M. V. Malyshev and V. M. Donnelly, *J. Appl. Phys.* **87**, 1642 (2000).
- ³¹G. R. Tynan, *J. Appl. Phys.* **86**, 5356 (1999).
- ³²V. A. Godyak, R. B. Piejak, and B. M. Alexandrovich, *Plasma Sources Sci. Technol.* **1**, 36 (1992).
- ³³H. Singh and D. B. Graves, *J. Appl. Phys.* **87**, 4098 (2000).